ACS APPLIED MATERIALS & INTERFACES

Research Article

www.acsami.org

Separation of Microcystin-LR by Cyclodextrin-Functionalized Magnetic Composite of Colloidal Graphene and Porous Silica

Arjyabaran Sinha and Nikhil R. Jana*

Centre for Advanced Materials, Indian Association for the Cultivation of Science, Kolkata-700032, India

Supporting Information

ABSTRACT: Microcystin-LR belongs to the family of microcystins produced by cyanobacteria and known to be the most toxic of this family. Existence of cyanobacteria in water bodies leads to the contamination of drinking water with microcystin-LR and thus their separation is essential for an advanced water purification system. Here we report functional nanocomposite-based selective separation of microcystin-LR from contaminated water. We have synthesized cyclodextrin-functionalized magnetic composite of colloidal graphene and porous silica where the cyclodextrin component offers host−guest interaction with microcystin-LR and the magnetic component offers easier separation of microcystin-LR from water. High surface area and large extent of chemical functional groups offer high loading (up to 18 wt %) of cyclodextrin with these nanocomposites, and the dispersible form of the nanocomposite offers easier accessibility of cyclodextrin to microcystin-LR. We have shown that microcystin-LR separation efficiency is significantly enhanced after functionalization with cyclodextrin, and among all the tested cyclodextrins, γ-cyclodextrin offers the best performance. We have also found that graphene-based nanocomposite offers better performance over porous silica-based nanocomposite due to better accessibility of cyclodextrins for interaction with microcystin-LR. The proposed graphene-based functional nanocomposite is environment friendly, reusable, and applicable for advanced water purification.

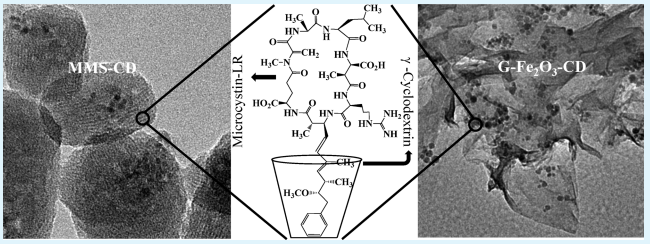

KEYWORDS: *microcystin-LR, graphene, cyclodextrin, nanoparticle, water purification*

INTRODUCTION

Microcystins are cyclic heptapeptides produced by cyanobacteria.[1,2] Among the microcystins family, the microcystin-LR is known to be most toxic.[3] As the cyanobacterial algal blooms in various water bodies are a worldwide issue, the contamination of drinking water by microcystins-LR and selective separation from contaminated water becomes a critical issue for advanced water purification technology.[1−5] Microcystins exists in several forms due to the variation of amino acids, and the presence of the hydrophobic Adda (3-amino-9-methoxy-2,6,8-trimethyl-10-phenyldeca-4,6-dienoic acid) moiety, which is the key component that binds with protein phosphatase to exhibit their toxicological activity.[6,7] Microcystin-LR is reported to induce acute and chronic toxicity to animals and humans.[1−3,8−11] Exposure to microcystin-LR causes diarrhea, vomiting, piloerection, and weakness, and all these toxic effects lead to liver damage.[1−3,8,9] In addition it is shown that microcystin-LR promotes tumor growth.[12,13]According to WHO guidelines the permissible limit of microcystin-LR in drinking water is 1.0 μg/liter.[2] Thus, separation/removal of microcystin-LR from drinking water is a very challenging issue.

Removal of microcystin-LR is challenging due to their high stability and resistance against chemical hydrolysis and oxidation.[14] Several traditional methods such as filtration, coagulation, flocculation, sedimentation, oxidation, and biological treatment have been investigated.[15] Conventional filtration, coagulation, flocculation, and sedimentation are effective for separation of cyanobacterial cells but ineffective for the separation of dissolved cyanotoxins.[16−18] Advanced oxidation methods such as chlorination and ozonation can remove cyanotoxin but require high dosage which causes other toxic side products.[19,20] Biological treatments are a less efficient and time-consuming process.[21] Photocatalytic degradation of microcystin is shown to be effective but not cost-effective and tested only on the laboratory scale.[22−24] In contrast adsorption based separation[25] is most effective for removal of toxic pollutants from water, and activated carbon[26] is most widely used for this purpose. However, activated carbon-based separation of microcystin is limited due to small micropores in carbon that cannot accommodate the large microcystin molecule. Recently, mesoporous carbon,[27,28] mesoporous silica,[29−32] and bare graphene oxide (GO)[33] have been used for the separation of microcystins. Although separation efficiency can be largely improved, all these materials do not exhibit selective separation of microcystin-LR.

Herein we report functional nanocomposites for selective separation of microcystin-LR from contaminated water. We have synthesized the magnetic composite of colloidal graphene and porous silica and then functionalized with cyclodextrin, which offers host−guest interaction with microcystin-LR. The

Received: March 7, 2015
Accepted: April 23, 2015
Published: April 23, 2015

DOI: 10.1021/acsami.5b02038
ACS Appl. Mater. Interfaces 2015, 7, 9911−9919

high surface area of the nanocomposite offers high loading of cyclodextrin, the dispersible form of the nanocomposite offers easier accessibility of cyclodextrin to microcystin-LR, and the magnetic component offers easier separation of microcystin-LR. We have selected graphene and mesoporous silica as they are known to have high surface area and are widely used in biomedical[34−36] and water purification[37−46] application, and their magnetic composites have been used for improved separation[37−39] and other applications.[48,49] Cyclodextrin is selected for functionalization as it is known to selectively interact with a variety of small molecules via host−guest interaction,[34,50−54] and recently it has been shown to interact with microcystin-LR.[55] Cyclodextrin is a cyclic oligomer of glucose composed of six to eight glucose units and has a hydrophobic cavity at the center of its molecular arrangement.[50] The size of the hydrophobic cavity increases from α- and β- to γ-cyclodextrin. It is shown that the Adda moiety of microcystin-LR is involved in the host−guest interaction with cyclodextrin, and γ-cyclodextrin offers the most stable inclusion complex as compared to β- or α-cyclodextrin.[55] Here we show that cyclodextrin functionalized nanocomposite also shows a similar trend and offers enhanced performance in separation of microcystin-LR.

EXPERIMENTAL SECTION

Chemicals. Tetraethylorthosilicate (TEOS), [3-(2-aminoethylamino)propyl]trimethoxysilane (AEAPS), (3-glycidyloxypropyl)trimethoxysilane, tetramethylammonium hydroxide (25 wt %, in methanol), β-cyclodextrin (CD), graphite powder (<20 μm), and hydrazine hydrate (98%) were purchased from Sigma-Aldrich and used as received. α-Cyclodextrin, γ-cyclodextrin, amino-β-cyclodextrin, amino-γ-cyclodextrin, and 1-ethyl-3-(3-(dimethylamino)-propyl)carbodiimide hydrochloride (EDC) were purchased from TCI Chemicals and used as received. Microcystin-LR was purchased from Enzo Life Sciences. Cetyltrimethylammonium bromide (CTAB) was purchased from Alfa Aesar. *N*-Hydroxysuccinimide was purchased from Fluka. Ammonia (25 wt %), potassium permanganate ($KMnO_4$), and succinic anhydride were purchased from Merck.

Instrumentation. UV−visible absorption spectra were recorded on a Shimadzu UV-2550 spectrophotometer in a 1 cm quartz cell. N_2 adsorption−desorption isotherm was measured using a Quantachrome Autosorb-1C, and the BET method was used to determine the surface area using adsorption data. The pore-size distributions were analyzed by using nonlocal density functional theory (NLDFT). TEM image of the samples was captured using an FEI Technai G2 transmission electron microscope. The field emission scanning electron microscopy (FESEM) images of the sample were taken by a Supra 40, Carl Zeiss Pvt. Ltd. instrument. A superconducting quantum interference device (SQID) magnetometer was used for magnetic measurement study of the composite materials. XRD measurement of the samples was performed on a Bruker D8 Advance powder diffractometer, by using Cu Kα (λ = 1.54 Å) as the incident radiation. Fourier transform infrared (FTIR) spectrum of KBr powder-pressed pellets was obtained from PerkinElmer Spectrum 100 FTIR spectrometer. Thermogravimetric analysis of the sample was performed using a TA SDT Q600 instrument. The Raman spectrum was recorded using Agiltron R3000 Raman spectrometer with 785 nm excitation laser having 5 mW laser power and 10 s integration time. HPLC (Waters 515) equipped with SunFire C18 column and UV detector (Waters 2489) was used for determination of microcystin-LR.

Synthesis of Cyclodextrin Functionalized Magnetic Graphene Composite (G-Fe_2O_3-CD). Silica coated iron oxide nanoparticle solution with primary amine terminated functional groups is synthesized using our previously reported method,[56] and a stock solution was prepared with a concentration of 2 mg/mL. Graphene oxide (GO) was prepared from natural graphite powder by modified Hummer's method,[57] and colloidal solution was prepared with a concentration of 1 mg/mL. In a separate vial cyclodextrin solution was prepared with the concentration of 50 mg/mL. Next, 10 mL of GO solution was mixed with 10 mL of cyclodextrin solution followed by the addition of 200 μL of NH_3 solution (25 wt %) under stirring condition. After 30 min of stirring, 1 mL of silica coated γ-Fe_2O_3 solution was added, and the whole mixture was stirred for another 30 min. Next, 200 μL of hydrazine solution (98%) was added, and the temperature of the solution was increased to 70−80 °C and maintained for 4 h. The color of the solution gradually turns black along with the appearance of partial precipitation. Next, the reaction was stopped, and 0.5 mL of NaCl solution (~20 mg/mL) was added to precipitate the composite materials. The precipitate was washed several times with distilled water, and it was finally dispersed in water for further use.

Functionalization of G-Fe_2O_3 with α-, β-, or γ-cyclodextrin[53,54] was achieved following the same procedure with the use of respective cyclodextrins. Dextran functionalized G-Fe_2O_3 was synthesized following the same procedure except that dextran was used instead of cyclodextrin. Nonfunctionalized G-Fe_2O_3 was synthesized by the above procedure without using any cyclodextrin or dextran.

Synthesis of Cyclodextrin Functionalized Magnetic Mesoporous Silica (MMS-CD). At first 1 mL as-synthesized hydrophobic γ-Fe_2O_3 was purified by a well-known precipitation−redispersion method and dissolved in 1 mL chloroform. Next, 4 mL of aqueous CTAB solution (0.15 M) was added under stirring condition and heated to 50−60 °C. After a few minutes γ-Fe_2O_3 nanoparticles were transferred into the aqueous phase and chloroform was evaporated. In a separate vial 200 mg of amine functionalized γ-cyclodextrin was dissolved in 4 mL of dry dimethylformamide and mixed with 40 μL of (3-glycidyloxypropyl)trimethoxysilane and reacted overnight.

Next, 4 mL of aqueous γ-Fe_2O_3 solution was diluted to 40 mL by adding water and mixed with 600 μL of NaOH (1 M) solution. Next, 2 mL of ethanol solution of tetraethoxysilane [240 μL of tetraethoxysilane was mixed with 8 mL of ethanol] and 1 mL of dimethylformamide solution of cyclodextrin functionalized silane were added. Next, the whole solution was stirred for another 3 h, and particles were precipitated by adding excess ethanol. The particles were separated by centrifuge and washed with water and ethanol to remove unreacted reagents. Finally, the CTAB template was removed by the NH_4NO_3-based extraction method and stored for further use.

Functionalization of MMS with α- and γ-cyclodextrin was achieved following the same procedure with the use of respective cyclodextrins. Nonfunctionalized MMS was synthesized by the above procedure without using cyclodextrin functionalized silane.

Separation of Microcystin-LR. A stock solution of microcystin-LR with the concentration of 500 μg/mL was prepared by dissolving in methanol−water (1:9 v/v) solution. In a separate vial stock solutions of G-Fe_2O_3-CD and MMS-CD were prepared. Next, solution of G-Fe_2O_3-CD or MMS-CD was mixed with solution of microcystin-LR with varied concentration. The typical concentrations of G-Fe_2O_3-CD and MMS-CD were 0.05 and 1.0 mg/mL, respectively, and the final volume of water was 1.0 mL. The whole solution was stirred for 2 h, and then particles were separated by laboratory based bar magnet. The supernatant solution was used for estimation of the remaining microcystin-LR by UV−visible spectroscopy or HPLC.

HPLC-based analysis of microcystin-LR involved a C18 column and UV detector. Two solvent systems were prepared composed of 0.05% aqueous trifluoroacetic acid (solution A) and methanol (solution B). The elution gradient started at 70% of solution A that decreased to 30% after 12 min, and after 2 min of stability it was back to 70% of solution A within 15 min. The sample injection volume was 50 μL with the flow rate of 1.0 mL/min, and the wavelength was set to 239 nm for microcystin-LR estimation.

RESULTS AND DISCUSSION

Design and Synthesis of Cyclodextrin Functionalized Nanocomposites. We have selected cyclodextrin as it is known to form an inclusion complex with microcystin-LR via host−guest interaction.[55] In addition the size of the hydro-

DOI: 10.1021/acsami.5b02038
ACS Appl. Mater. Interfaces 2015, 7, 9911−9919

Scheme 1. Synthesis Strategies for Cyclodextrin Functionalized Magnetic Graphene Composite (G-Fe_2O_3-CD) and Cyclodextrin Functionalized Magnetic Mesoporous Silica (MMS-CD)

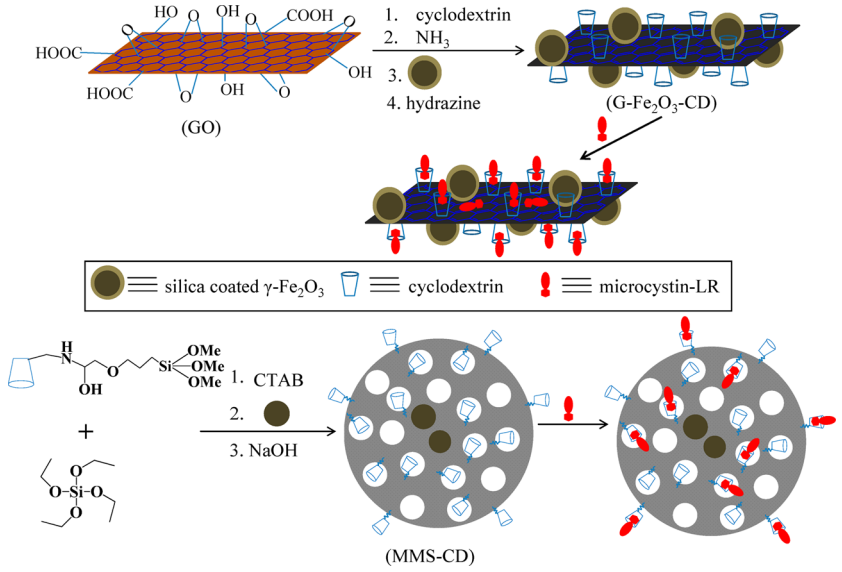

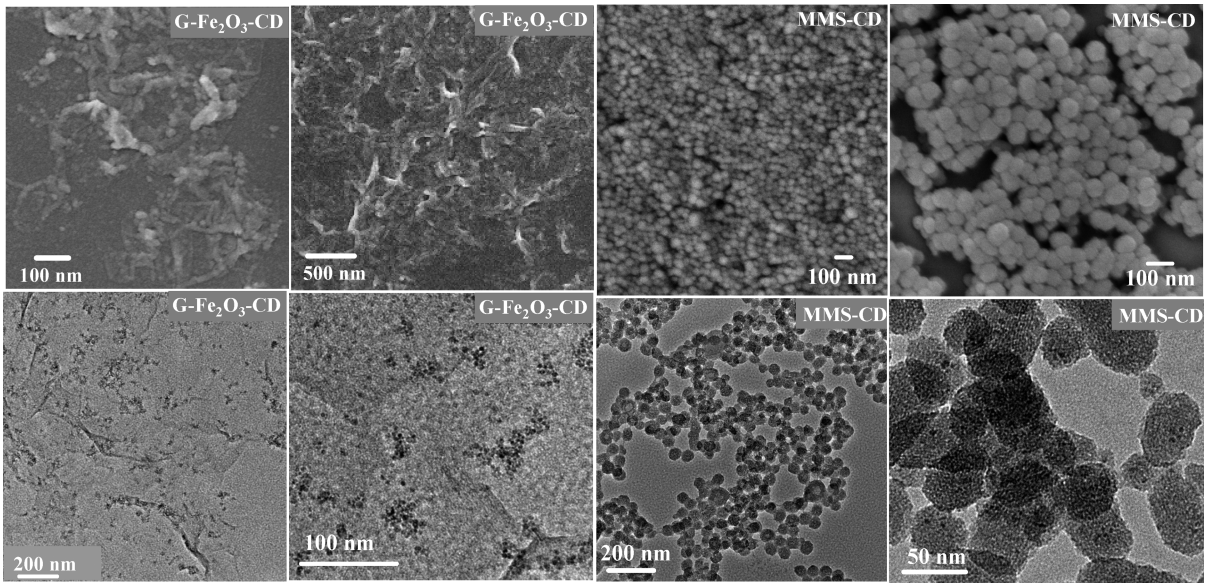

Figure 1. Low and high resolution SEM images (top panels) and TEM images (bottom panels) of G-Fe_2O_3-CD and MMS-CD.

phobic cavity, responsible for the inclusion complex, can be modulated by using commercially available α-, β-, or γ-cyclodextrin. All the cyclodextrins are chemically stable, water-soluble, and relatively cheap. Two different graphene and porous silica based materials are selected as they are known to have high surface area that can be used for high loading of cyclodextrins. Magnetic and colloidal forms of nanocomposite of graphene and porous silica are designed with the intention that colloidal forms are easily accessible by microcystin-LR and the magnetic property can be utilized for easier separation.

Synthesis approaches for cyclodextrin functionalized magnetic graphene composite (G-Fe_2O_3-CD) and cyclodextrin functionalized magnetic mesoporous silica (MMS-CD) are shown in Scheme 1. First, hydrophobic γ-Fe_2O_3 nanoparticle of 6−8 nm size is synthesized via high temperature degradation of iron stearate salt and then transformed into silica coated and primary amine terminated γ-Fe_2O_3 nanoparticle by the reported method.[56] Colloidal graphene oxide (GO) is synthesized via Hummer's method[57] and mixed with cyclodextrin and silica coated γ-Fe_2O_3 nanoparticles in the presence of ammonia. At this stage cyclodextrins are attached to the GO surface via hydrophobic or hydrogen bonding interaction and covalent bonding between the hydroxyl groups of cyclodextrin with the epoxy groups present on the GO surface.[53,54,58] The γ-Fe_2O_3 nanoparticles are attached onto the GO surface due to the electrostatic interaction between cationic γ-Fe_2O_3 nanoparticles and anionic GO and due to the reaction of the primary amine group on the γ-Fe_2O_3 nanoparticles surface with the epoxy groups of GO.[39] Next, GO is reduced by hydrazine with the formation of the G-Fe_2O_3-CD composite.

For the preparation of MMS-CD, amino cyclodextrin is reacted with epoxysilane and used as silane precursor for the synthesis of MMS.[59] In the resultant MMS-CD, cyclodextrin is covalently bound with the pores of MMS. Alternatively, the γ-

DOI: 10.1021/acsami.5b02038
ACS Appl. Mater. Interfaces 2015, 7, 9911−9919

Fe_2O_3 nanoparticle incorporated and primary amine terminated MMS is synthesized first, and then MMS-CD has been synthesized via EDC coupling between MMS and carboxylated cyclodextrin.[34]

Characterization of G-Fe_2O_3-CD and MMS-CD. SEM and TEM have been used to investigate the morphology and structure of as prepared G-Fe_2O_3-CD and MMS-CD nanocomposites (Figure 1). Graphene flake structures are observed in the SEM images of G-Fe_2O_3-CD. The TEM image clearly shows that γ-Fe_2O_3 nanoparticles of 6−8 nm sizes are attached with graphene surface. Similarly, SEM image clearly shows that the MMS-CDs are spherical in nature with the size range of 80−100 nm, and the TEM image shows the composite nature of MMS-CDs with the incorporated γ-Fe_2O_3 nanoparticles. XRD patterns of both composite materials exhibit reflections at 2θ = 30.658, 35.948, 43.558, 53.358, 57.588, and 63.228 due to (220), (311), (400), (422), (511), and (440) planes of γ-Fe_2O_3 which provide further evidence of the presence of γ-Fe_2O_3 nanoparticles (Supporting Information, Figure S1).

Magnetic measurement study of G-Fe_2O_3-CD and MMS-CD shows the characteristic hysteresis which almost disappears at room temperature, a feature commonly observed in superparamagnetic materials (Figure 2). The saturation magnetization values obtained for G-Fe_2O_3-CD are 8.16 and 5.43 emu g^{-1} at 10 K and 300 K, respectively. Similar saturation magnetization values for MMS-CD are 4.13 and 2.56 emu g^{-1} at 10 K and 300 K, respectively. Zero field-cooling (ZFC) and field-cooling (FC) magnetization curves of G-Fe_2O_3-CD and MMS-CD (measured at 200 Oe) display well-defined blocking temperatures of 20 K and 10 K, respectively, which also indicates the superparamagnetic nature of the nanocomposites.

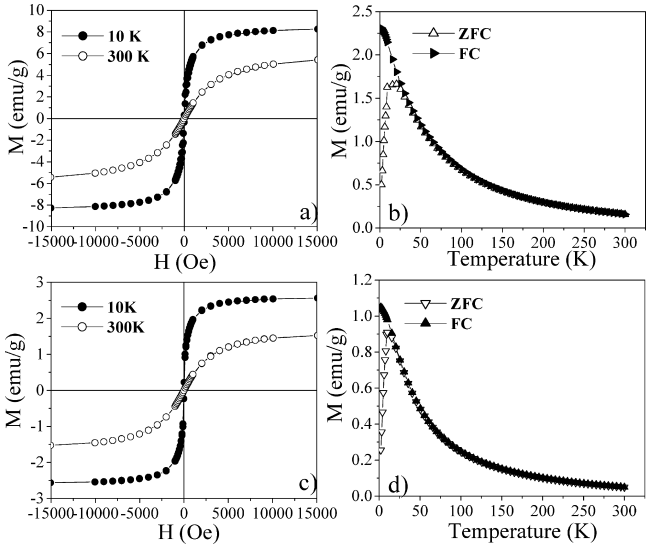

Figure 2. Field dependent magnetization curves at 10 and 300 K and the respective temperature dependent zero-field-cooled (ZFC) and field-cooled (FC) magnetization curves for G-Fe_2O_3-CD (a, b) and MMS-CD (c, d).

The porous structure of nanocomposites has been investigated before functionalization with cyclodextrin via N_2 adsorption−desorption isotherm. G-Fe_2O_3 shows the type-IV adsorption−desorption isotherm with BET surface area of 400 m^2/g and pore volume of 0.28 cm^3/g[38,39] (Supporting Information, Figure S2). Similarly, MMS shows the type-IV adsorption isotherm which is commonly observed for mesoporous materials with the surface area in the range of 300−400 m^2/g and pore volume of 0.21−0.3 cm^3/g.[34] However, the surface area decreases to 30−50 m^2/g after modification with cyclodextrin due to extensive coverage of the surface by cyclodextrins.

Functionalization with cyclodextrin is confirmed from FTIR study, and the extent of functionalization has been estimated by thermogravimetric analysis (Figure 3). FTIR spectra of G-Fe_2O_3-CD and MMS-CD show a typical characteristic vibration band of cyclodextrin. For example, vibrational bands of cyclodextrin are observed for G-Fe_2O_3-CD at 1024, 1648, and 2924 cm^{-1} due to coupled C—O/C—C stretching/O—H bending vibrations, HOH vibration of hydroxyl group, and CH_2 stretching vibration, respectively.[53,54] Similarly, vibration bands are observed for MMS-CD at 1562 and 1730 cm^{-1} which are characteristic of N—H bending vibration and C═O stretching vibration[34](Supporting Information, Figure S3). The amount of cyclodextrin attached with MMS and G-Fe_2O_3 is estimated from thermogravimetric analysis. All the TGA curves of MMS, MMS-CD, G-Fe_2O_3, and G-Fe_2O_3-CD show small weight loss at <100 °C due to adsorbed water and significant weight loss between 250 to 400 °C due to the degradation of organic mass. However, MMS-CD and G-Fe_2O_3-CD show ∼15−18% extra weight loss (as compared to MMS and G-Fe_2O_3) at 250 to 400 °C which is due to the degradation of the attached cyclodextrin functional group (Figure 3b,c). Thus, thermogravimetric analysis results indicate that about 15−18 wt % of cyclodextrin is present in G-Fe_2O_3-CD and MMS-CD. Elemental analysis shows that the C:H:N weight ratio changes from 8:2.3:0.5 to 18:3.5:0.8 after the MMS is functionalized with γ-cyclodextrin. This result further corroborates that 18−20 wt % γ-cyclodextrin is attached with MMS.

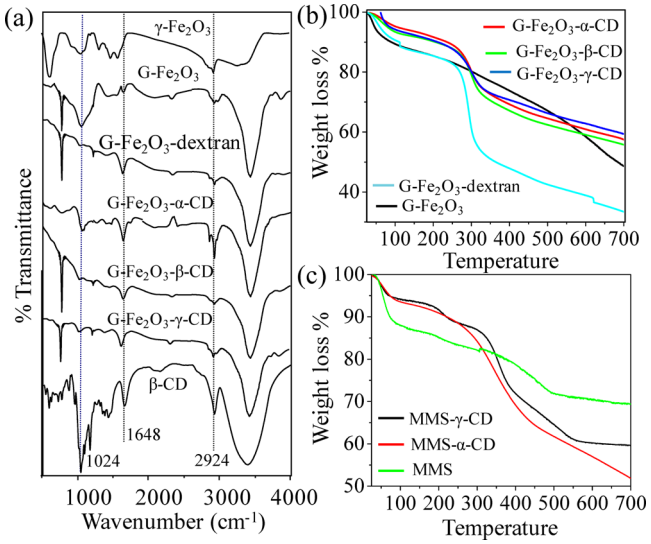

Figure 3. (a) FTIR spectra of G-Fe_2O_3-CD along with different control samples. Results show the appearance of characteristic vibration bands of cyclodextrin corresponding at 1024, 1648, and 2924 cm^{-1} (highlighted by the dotted line) after functionalization. (b) TGA curves of G-Fe_2O_3 before and after functionalization with cyclodextrin and dextran. 15−30% weight loss in the temperature range of 260−350 °C is due to the cyclodextrin/dextran functionalization. (c) TGA graph of MMS before and after cyclodextrin functionalization, showing the 15% weight loss in the temperature range of 290 to 400 °C due to the cyclodextrin functionalization.

DOI: 10.1021/acsami.5b02038
ACS Appl. Mater. Interfaces 2015, 7, 9911−9919

The Raman spectrum of G-Fe_2O_3-CD before and after cyclodextrin functionalization shows two well documented D and G bands of graphene at about 1305 and 1600 cm^{-1}, attributed due to the disorder in carbon atoms and SP^2 in-plane vibration of carbon atoms, respectively (Supporting Information, Figure S4). The intensity ratio of D band to G band increases after cyclodextrin functionalization, demonstrating the influence of functionalization to the structural distortion of graphene.

Separation of Microcystin-LR by G-Fe_2O_3-CD and MMS-CD. Advantage of cyclodextrin functionalized nanocomposites toward separation of microcystin-LR from water has been investigated in detail. Figure 4, Table 1, and

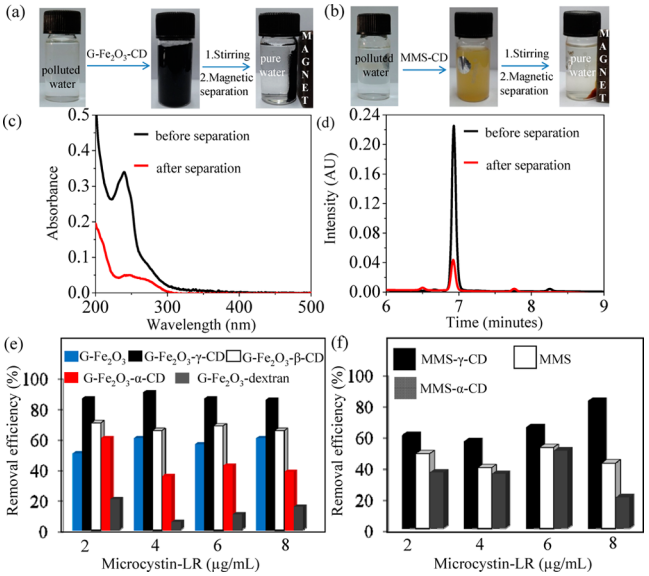

Figure 4. (a, b) Separation of microcystin-LR from water using G-Fe_2O_3-CD (a) and MMS-CD (b). (c) Typical UV−visible absorption spectra of microcystin-LR solution before and after treatment with G-Fe_2O_3-CD. (d) HPLC chromatogram of microcystin-LR solution before and after treatment with MMS-CD. (e) Removal efficiency of microcystin-LR using G-Fe_2O_3-CD and other functional G-Fe_2O_3. The concentration of nanocomposite has been kept at 0.05 mg/mL. (f) Removal efficiency of microcystin-LR using MMS-CD and other functional MMS. The concentration of nanocomposite has been kept at 1.0 mg/mL.

Supporting Information Figures S5−S8 show the separation approach and removal efficiency of microcystin-LR by different nanocomposites. Typically, G-Fe_2O_3-CD or MMS-CD nanocomposite is mixed with the aqueous solution of microcystin-LR and then the nanocomposite is removed by magnet. Next, the amount of remaining microcystin-LR in water has been estimated using HPLC or UV−visible spectroscopy. Digital images in Figure 4a show the response of colloidal solution of nanocomposites by laboratory-based bar magnet that attracts them, leaving the clear bulk solution. This property of the material helps easier separation of adsorbed materials. We have determined removal efficiency for G-Fe_2O_3-CD and MMS-CD, keeping the fixed concentration of microcystin-LR (6 μg/mL), and then selected an optimum concentration of each material for microcystin-LR separation (Supporting Information, Figure S5). The results indicate that MMS-CD is less efficient than G-Fe_2O_3-CD, and so more MMS-CD is needed for separation of a similar amount of microcystin-LR separation. Thus, we have selected some optimum concentration of each material for microcystin-LR separation. Typical analysis results are shown in Figure 4c,d. It shows that absorbance and HPLC signal of microcystin-LR decreases remarkably after treatment with nanocomposites. Each separation experiment has been repeated three times, and average values are shown in Figure 4e,f with ∼10% error. The results summarize the separation efficiencies due to different functionalization. The results show that microcystin-LR can be separated without any functionalization which is due to nonspecific adsorption with nanocomposites. However, separation performance is greatly enhanced after functionalization with cyclodextrin, and among all the cyclodextrins, the γ-cyclodextrin offers the best performance. Such best performance by γ-cyclodextrin over α- and β-cyclodextrin is attributed to the most stable inclusion complex formation between γ-cyclodextrin and the Adda moiety of microcystin-LR.[55] Interestingly dextran functionalization significantly decreases the removal efficiency of microcystin-LR which implies that dextran significantly reduces the nonspecific binding of microcystin-LR with nanocomposites.

Microcystin-LR separation efficiencies by G-Fe_2O_3-CD and MMS-CD have been compared, and it is observed that G-Fe_2O_3-CD offers better performance as compared to MMS-CD (Table 1 and Figure 4). For example, separation of similar concentration of microcystin-LR with the separation efficiency of >60% requires ∼20 times of MMS-CD as compared to G-Fe_2O_3-CD (Figure 4e,f). However, enhancement of separation performance after functionalization with γ-cyclodextrin is also observed in the case of MMS-CD. Removal capacity has been summarized for different nanocomposites. The values are in the range of 4−8 mg/g for MMS and MMS-CD and in the range 80−160 mg/g for G-Fe_2O_3 and G-Fe_2O_3-CD. The dextran functionalization of G-Fe_2O_3 significantly decreases the removal capacity to 10 mg/g as it decreases the nonspecific binding. It is interesting to note that although similar percent of cyclodextrin is present in both nanocomposites, the G-Fe_2O_3-CD performs better than the MMS-CD. This may be due to the nonaccessibility of large molecular weight microcystin-LR to each of the MMS-bound cyclodextrin. In particular the cyclodextrins that are bound inside the pores are not easily

Table 1. Removal Capacity of Different Nanocomposites with Respect to Weight Percent of Cyclodextrin Present

		weight % cyclodextrin (CD)			removal capacity[b] (mg/g) after being functionalized with			
materials	surface area[a] (m^2/g)	α-CD	β-CD	γ-CD	α-CD	β-CD	γ-CD	----
G-Fe_2O_3-CD	400(30)	17	18	16	80	140	160	120
MMS-CD	300(50)	19	---	17	4	-----	8	5

[a]Surface area is determined before functionalization with cyclodextrin. The value within parentheses indicates the surface area after being functionalized with γ-cyclodextrin. [b]Removal capacity is defined by milligram (mg) of microcystin-LR removed per gram (g) of materials. It is determined from the initial concentration (C_0) and final concentrations (C_f) of microcystin-LR after treatment with nanocomposite, solution volume (V), and mass of nanocomposite (m) according to the following equation: removal capacity = $(C_0 - C_f)V/m$.

DOI: 10.1021/acsami.5b02038
ACS Appl. Mater. Interfaces 2015, 7, 9911−9919

accessible to microcystin-LR. In contrast graphene has a flat surface and thus all the cyclodextrins are accessible to microcystin-LR. So the high performance of microcystin-LR separation by G-Fe_2O_3-CD is mainly due to high loading of cyclodextrin and the flat surface of graphene with dispersible property that offers easier accessibility to microcystin-LR.

One of the most important aspects for practical application is if the materials can be regenerated and reused. This has been tested for removal of microcystin-LR using G-Fe_2O_3-γ-CD as representative material (Figure 5). Detailed procedures of G-

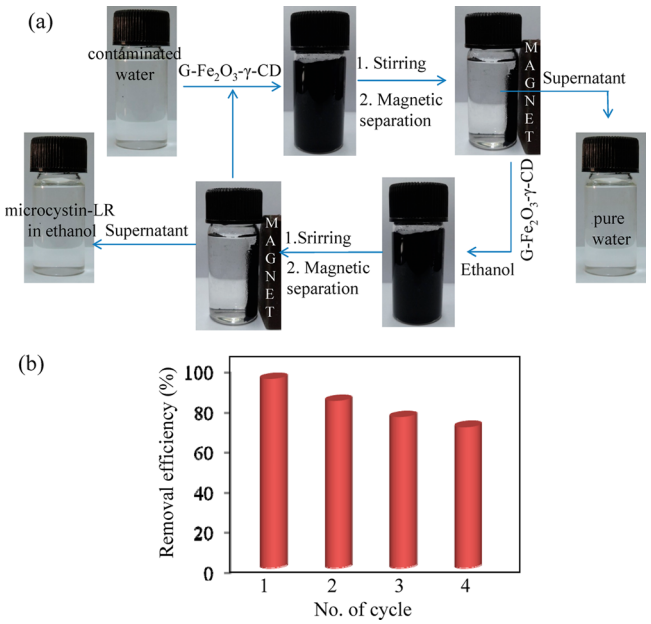

Figure 5. (a) Schematic representation of G-Fe_2O_3-γ-CD-based microcystin-LR separation and regeneration of G-Fe_2O_3-γ-CD for repeated use. (b) Microcystin-LR removal efficiency using successively reused G-Fe_2O_3-γ-CD. Typically, 0.25 mg of G-Fe_2O_3-γ-CD and 5 mL of fresh microcystin-LR solution (5 μg/mL) have been used in this recycling experiment.

Fe_2O_3-γ-CD-based microcystin-LR separation and regeneration of G-Fe_2O_3-γ-CD for repeated use are shown in Figure 5a. Regeneration of G-Fe_2O_3-γ-CD involves magnetic separation followed by repeated washing with ethanol to extract the adsorbed microcystin-LR. Results show that G-Fe_2O_3-γ-CD can be used several times with little loss of removal efficiency. The loss of removal efficiency can be due to aggregation of G-Fe_2O_3-γ-CD and detachment of some cyclodextrins during regeneration steps or poor microcystin-LR removal via regeneration steps. It is also important that the materials should be environmentally friendly or nontoxic so that it does not introduce any secondary pollutant during the removal of microcystin-LR. In order to prove the nontoxic and environmentally friendly nature of G-Fe_2O_3-CD, the cell viability study has been performed using Chinese hamster ovary (CHO) cell as representative. Results show that about 80% of the cells are viable after 24 h of incubation with G-Fe_2O_3-CD, suggesting that the material is nontoxic and environmentally friendly (Supporting Information, Figure S8) .

Selective separation performance of microcystin-LR from contaminated water has been investigated via separating microcystin-LR in the presence of natural organic matter[60] and metal ions (Figure 6). Natural organic matter and metal

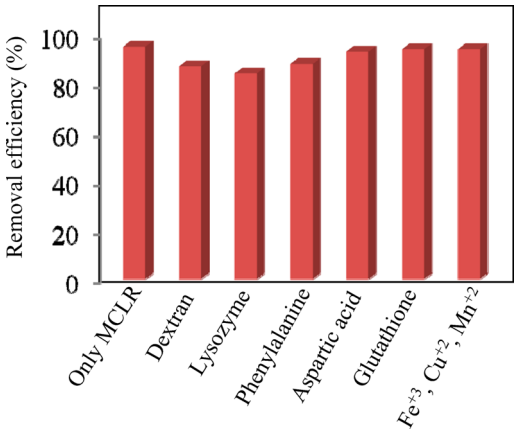

Figure 6. Removal efficiency of microcystin-LR by G-Fe_2O_3-γ-CD in the presence of natural organic matter and metal ions. Experimental conditions: 0.1 mg of G-Fe_2O_3-γ-CD is added to 2 mL of microcystin-LR (concentration 5 μg/mL) solution in the presence of different natural organic matter or metal ions (concentration 20 μg/mL) and is stirred for 2 h at room temperature, prior to the magnetic separation.

ions are present in most of the surface, ground, and soil waters, and they have negative effect on the removal efficiency of microcystin-LR. We have used a variety of natural organic matter such as different amino acid, protein (lysozyme), and polysaccharide (dextran) with the concentration of 20 μg/mL and different metal ions with the concentration of 20 μg/mL. We have observed that removal efficiency of microcystin-LR by G-Fe_2O_3-γ-CD is reasonably unaffected in the presence of natural organic matter and metal ions. This result reveals that G-Fe_2O_3-γ-CD can selectively separate microcystin-LR from the contaminated water without significant loss of removal efficiency.

Functional Magnetic Graphene-Based Efficient Separation of Microcystin-LR. The high surface area of graphene has inspired researchers for adsorption based separation application. These applications include separation of toxic metal ions and organic pollutants. For example, ethylenediaminetetraacetic acid functionalized GO[40] has been used for separation of Pb(II) from water with removal capacity of 480 mg/g, thiol functionalized GO[41] has been used for the separation of Hg(II) from water with removal capacity of 200 mg/g, polypyrrol-reduced GO[42] has been used for separation of Hg(II) with removal capacity of 980 mg/g, ethylenediamine functionalized reduced graphene oxide[43] has been used for Cr(VI) separation, and polydopamine and polyacrylamide functionalized graphene[44,45] have been used for the separation of toxic metal ions. Sulfonated graphene[46] has been reported for separation of organic pollutants with removal capacity up to 347 mg/g, polydopamine and polyacrylamide functionalized graphenes[44,45] are reported for the separation of organic dye, and hydrophobic polymer grafted GO[47] has been used for separation of tetrabromobisphenol A with removal capacity of 22 mg/g. Here we have used cyclodextrin functionalized magnetic graphene for separation of microscystin-LR with the removal capacity up to 160 mg/g.

Various nanomaterials are under development for the separation of microcystin-LR with the focus of enhanced removal efficiency and improved selectivity. For example, mesoporous silica-based materials have been reported for the adsorption based separation of microcystin-LR with the removal capacity of 6−13 mg/g.[29−32] Bare GO has been used

DOI: 10.1021/acsami.5b02038
ACS Appl. Mater. Interfaces 2015, 7, 9911−9919

for separation of microcystin-LR with the removal capacity of 17 mg/g.[33] This lower removal capacity by GO is due to low hydrophobic interaction between GO and microcystin-LR and electrostatic repulsion between negatively charged GO and anionic groups of the microcystin-LR. TiO_2 coated magnetic graphene has been investigated for the separation and UV light dependent photocatalytic degradation of microcystin-LR.[24] Recently, mesoporous carbon materials with bimodal mesopores of 2.8 and 5.8 nm have been synthesized for adsorption based separation of microcystin-LR with removal capacity of 526 mg/g.[27,28] This high removal capacity of mesoporous carbon arises due to the high surface area, varied pore architectures, and hydrophobic surface of mesoporous carbon. In contrast the presented G-Fe_2O_3-γ-CD offers selective binding of microcystin-LR with the hydrophobic cavity of cyclodextrin. In addition, Fe_2O_3 nanoparticles present on the composite materials inhibit the graphene−graphene aggregation and further increase the adsorption site for microcystin-LR.[39] Compared to the reported nanomaterials, the presented G-Fe_2O_3-γ-CD has four distinct advantages. First, G-Fe_2O_3-γ-CD is dispersible in water, and cyclodextrins are attached on the flat surface of graphene. As a result cyclodextrins are easily accessible for binding with microcystin-LR. Second, γ-Fe_2O_3 component in G-Fe_2O_3-γ-CD offers easier magnetic separation option of adsorbed microcystin-LR. Third, high surface area of graphene offers high loading of cyclodextrin on the graphene surface. Fourth, G-Fe_2O_3-γ-CD can selectively remove microcystin-LR from the water in the presences of natural organic matter and metal ions.

CONCLUSION

In summary, we have synthesized graphene and porous silica-based magnetic nanocomposites which are functionalized with cyclodextrin. These functional nanocomposites have been used for separation of microcystin-LR from contaminated water via host−guest interaction between microcystin-LR and cyclodextrin. High surface area and large extent of chemical functional groups offer high loading (up to 18%) of cyclodextrin with nanocomposites. Resultant functional nanocomposites are dispersible in water but separable by external magnet. Microcystin-LR separation efficiency is significantly enhanced after functionalization with cyclodextrin, and among all the tested cyclodextrins, γ-cyclodextrin functionalization offers best performance. Among the two functional nanocomposites, graphene-based composites offer better performance over porous silica-based composite as most of the cyclodextrins are accessible for interaction with microcystin-LR. The proposed graphene-based functional nanocomposite is environmentally friendly and can be reused. Developed functional nanomaterials can be used for advanced water purification applications.

ASSOCIATED CONTENT

Supporting Information

Details of characterization of mesoporous materials, functional characterization, adsorption isotherm of microcystin-LR on G-Fe_2O_3-γ-CD, cell viability study in the presence of G-Fe_2O_3-CD. The Supporting Information is available free of charge on the ACS Publications website at DOI: 10.1021/acsami.5b02038.

AUTHOR INFORMATION

Corresponding Author

*E-mail: camnrj@iacs.res.in. Telephone: +91-33-24734971. Fax: +91-33-24732805.

Notes

The authors declare no competing financial interest.

ACKNOWLEDGMENTS

Authors acknowledge CSIR and DST, government of India, for financial assistance. AS acknowledges CSIR, India, for research fellowships.

REFERENCES

(1) de Figueiredo, D. R.; Azeiteiro, U. M.; Esteves, S. M.; Gonblves, F. J. M.; Pereira, M. J. Microcystin Producing Blooms a Serious Global Public Health Issue. *Ecotoxicol. Environ. Saf.* **2004**, *59*, 151−163.

(2) *Cyanobacterial Toxins: Microcystin-LR in Drinking-Water*; World Health Organization: Geneva, 1998.

(3) Dawson, R. M. The Toxicology of Microcystin. *Toxicon* **1998**, *36*, 953−962.

(4) Hoegera, S. J.; Hitzfeldb, B. C.; Dietrich, D. R. Occurrence and Elimination of Cyanobacterial Toxins in Drinking Water Treatment Plants. *Toxicol. Appl. Pharmacol.* **2005**, *203*, 231−242.

(5) Schwarzenbach, R. P.; Escher, B. P.; Fenner, K.; Hofstetter, T. B.; Johnson, C. A.; Gunten, U. V.; Wehrli, B. The Challenge of Micropollutants in Aquatic Systems. *Science* **2006**, *313*, 1072−1077.

(6) MacKintoshl, C.; Beatti, K. A.; Klumpp, S.; Cohen, P.; Codd, G. A. Cyanobacterial Microcystin-LR is a Potent and Specific Inhibitor of Protein Phosphatases 1 and 2A from Both Mammals and Higher Pants. *FEBS Lett.* **1990**, *264*, 187−192.

(7) Runnegar, M. T.; Kong, S.; Berndt, N. Protein Phosphatase Inhibition and In Vivo Hepatotoxicity of Microcystins. *Am. J. Physiol.* **1993**, *265*, G224−230.

(8) Codd, G. A.; Morrison, L. F.; Metcalf, J. S. Cyanobacterial Toxins: Risk Management for Health Protection. *Toxicol. Appl. Pharmacol.* **2005**, *203*, 264−272.

(9) Briand, J. F.; Jacquet, S.; Bernard, C.; Humbert, J. F. Health Hazards for Terrestrial Vertebrates from Toxic Cyanobacteria in Surface Water Ecosystems. *Vet. Res.* **2003**, *34*, 361−377.

(10) Jasionek, G.; Zhdanov, A.; Davenport, J.; Blaha, L.; Papkovsky, D. B. Mitochondrial Toxicity of Microcystin-LR on Cultured Cells: Application to the Analysis of Contaminated Water Samples. *Environ. Sci. Technol.* **2010**, *44*, 2535−2541.

(11) Li, X.; Zhao, Q.; Zhou, W.; Xu, L.; Wang, Y. The Effects of Chronic Exposure to Microcystin-LR on Hepatocyte Mitochondrial DNA Replication in Mice. *Environ. Sci. Technol.* **2015**, *49*, 4665−4672.

(12) Matsushima, R. N.; Ohta, T.; Nishiwaki, S.; Suganuma, M.; Kohyama, K.; Ishikawa, T.; Carmichael, W. W.; Fujiki, H. Liver Tumor Promotion by the Cyanobacterial Cyclic Peptide Toxin Microcystin-LR. *J. Cancer Res. Clin. Oncol.* **1992**, *118*, 420−424.

(13) Christen, V.; Meili, N.; Fent, K. Microcystin-LR Induces Endoplasmatic Reticulum Stress and Leads to Induction of NF κB, Interferon-Alpha and Tumor Necrosis Factor-Alpha. *Environ. Sci. Technol.* **2013**, *47*, 3378−3385.

(14) Song, W.; De La Cruz, A. A.; Rein, K.; O'Shea, K. E. Ultrasonically Induced Degradation of Microcystin-LR and -RR: Identification of Products, Effect of pH, Formation and Destruction of Peroxides. *Environ. Sci. Technol.* **2006**, *40*, 3941−3946.

(15) Lawton, L. A.; Robertson, P. K. J. Physico-Chemical Treatment Methods for the Removal of Microcystins (Cyanobacterial Hepatotoxins) from Potable Waters. *Chem. Soc. Rev.* **1999**, *28*, 217−224.

(16) Teixeira, M. R.; Rosa, M. J. Microcystins Removal by Nanofiltration Membranes. *Sep. Purif. Technol.* **2005**, *46*, 192−201.

(17) Yuana, B. L.; Qua, J. H.; Fu, M. L. Removal of Cyanobacterial Microcystin-LR by Ferrate Oxidation−Coagulation. *Toxicon* **2002**, *40*, 1129−1134.

DOI: 10.1021/acsami.5b02038
ACS Appl. Mater. Interfaces 2015, 7, 9911−9919

(18) Wu, X.; Xiao, B.; Li, R.; Wang, C.; Huang, J.; Wang, Z. Mechanisms and Factors Affecting Sorption of Microcystins onto Natural Sediments. *Environ. Sci. Technol.* **2011**, *45*, 2641−2647.
(19) Rodriguez, E.; Onstad, G. D.; Kull, T. P. J.; Metcalf, J. S.; Acero, J. L.; Gunten, U. V. Oxidative Elimination of Cyanotoxins: Comparison of Ozone, Chlorine, Chlorine Dioxide and Permanganate. *Water Res.* **2007**, *41*, 3381−3393.
(20) Kronberg, L.; Vartiainen, T. Ames Mutagenicity and Concentration of the Strong Mutagen Chloro-4-(Dichloromethyl)-5-Hydroxy-2(5H)-Furanone and of Its Geometric Isomer E-2-Chloro-3-(Dichloromethyl)-4-Oxobutenoic Acid in Chlorine-Treated Tap Waters. *Mutat. Res. Genet. Toxicol.* **1988**, *206*, 177−1821.
(21) Bournea, D. G.; Blakeleyb, R. L.; Riddlesc, P.; Jones, G. J. Biodegradation of the Cyanobacterial Toxin Microcystin LR in Natural Water and Biologically Active Slow Sand Filters. *Water Res.* **2006**, *40*, 1294−1302.
(22) Pelaez, M.; Baruwati, B.; Varma, R. S.; Luque, R.; Dionysiou, D. D. Microcystin-LR Removal from Aqueous Solutions Using a Magnetically Separable N-doped TiO_2 Nanocomposite Under Visible Light Irradiation. *Chem. Commun.* **2013**, *49*, 10118−10120.
(23) Long, T. C.; Saleh, N.; Tilton, R. D.; Lowry, G. V.; Veronesi, B. Titanium Dioxide (P25) Produces Reactive Oxygen Species in Immortalized Brain Microglia (BV2): Implications for Nanoparticle Neurotoxicity. *Environ. Sci. Technol.* **2006**, *40*, 4346−4352.
(24) Liang, Y. L.; He, X. W.; Chen, L. X.; Zhang, Y. K. Preparation and Characterization of TiO_2−Graphene@Fe_3O_4 Magnetic Composite and Its Application in the Removal of Trace Amounts of Microcystin-LR. *RSC Adv.* **2014**, *4*, 56883−56891.
(25) Wu, Z.; Zhao, D. Ordered Mesoporous Materials as Adsorbents. *Chem. Commun.* **2011**, *47*, 3332−3338.
(26) Huang, W. J.; Cheng, B. L.; Cheng, Y. L. Adsorption of Microcystin- LR by Three Types of Activated Carbon. *J. Hazard. Mater.* **2007**, *141*, 115−122.
(27) Zhang, X.; Jiang, L. Fabrication of Novel Rattle-Type Magnetic Mesoporous Carbon Microspheres for Removal of Microcystins. *J. Mater. Chem.* **2011**, *21*, 10653−10657.
(28) Teng, W.; Wu, Z.; Fan, J.; Chen, H.; Feng, D.; Lv, Y.; Wang, J.; Asiri, A.; Zhao, M. D. Ordered Mesoporous Carbons and Their Corresponding Column for Highly Efficient Removal of Microcystin-LR. *Energy Environ. Sci.* **2013**, *6*, 2765−2776.
(29) Teng, W.; Wu, Z.; Feng, D.; Fan, J.; Wang, J.; Wei, H.; Song, M.; Zhao, D. Rapid and Efficient Removal of Microcystins by Ordered Mesoporous Silica. *Environ. Sci. Technol.* **2013**, *47*, 8633−8641.
(30) Chen, H.; Lu, X.; Deng, C.; Yan, X. Facile Synthesis of Uniform Microspheres Composed of a Magnetite Core and Copper Silicate Nanotube Shell for Removal of Microcystins in Water. *J. Phys. Chem. C* **2009**, *113*, 21068−21073.
(31) Lu, X.; Liu, H.; Deng, C.; Yan, X. Facile Synthesis and Application of Mesoporous Silica Coated Magnetic Carbon Nanotubes. *Chem. Commun.* **2011**, *47*, 1210−1212.
(32) Deng, Y.; Qi, D.; Deng, C.; Zhang, X.; Zhao, D. Superparamagnetic High-Magnetization Microspheres with an Fe_3O_4@SiO_2 Core and Perpendicularly Aligned Mesoporous SiO_2 Shell for Removal of Microcystins. *J. Am. Chem. Soc.* **2008**, *130*, 28−29.
(33) Pavagadhi, S.; Tang, A. L. L.; Sathishkumar, M.; Loh, K. P.; Balasubramanian, R. Removal of Microcystin-LR and Microcystin-RR by Graphene Oxide: Adsorption and Kinetic Experiments. *Water Res.* **2013**, *47*, 4621−4629.
(34) Sinha, A.; Basiruddin, S.; Chakraborty, A.; Jana, N. R. β-Cyclodextrin Functionalized Magnetic Mesoporous Silica Colloid for Cholesterol Separation. *ACS Appl. Mater. Interfaces* **2015**, *7*, 1340−1347.
(35) Li, Z.; Barnes, J. C.; Bosoy, A.; Stoddart, J. F.; Zink, J. I. Mesoporous Silica Nanoparticles in Biomedical Applications. *Chem. Soc. Rev.* **2012**, *41*, 2590−2605.
(36) Chung, C.; Kim, Y. K.; Shin, D.; Ryoo, S. R.; Hong, B. H.; Min, D. H. Biomedical Applications of Graphene and Graphene Oxide. *Acc. Chem. Res.* **2013**, *46*, 2211−2224.
(37) Sinha, A.; Jana, N. R. Functional, Mesoporous, Superparamagnetic Colloidal Sorbents for Efficient Removal of Toxic Metals. *Chem. Commun.* **2012**, *48*, 9272−9274.
(38) Geng, Z.; Lin, Y.; Yu, X.; Shen, Q.; Ma, L.; Li, Z.; Pan, N.; Wang, X. Highly Efficient Dye Adsorption and Removal: a Functional Hybrid of Reduced Graphene Oxide−Fe_3O_4 Nanoparticles As an Easily Regenerative Adsorbent. *J. Mater. Chem.* **2012**, *22*, 3527−3535.
(39) Sinha, A.; Jana, N. R. Graphene-Based Composite with γ-Fe_2O_3 Nanoparticle for the High-Performance Removal of Endocrine-Disrupting Compounds from Water. *Chem.—Asian J.* **2013**, *8*, 786−791.
(40) Madadrang, C. J.; Kim, H. Y.; Gao, G.; Wang, N.; Zhu, J.; Feng, H.; Gorring, M.; Kasner, M. L.; Hou, S. Adsorption Behavior of EDTA-Graphene Oxide for Pb (II) Removal. *ACS Appl. Mater. Interfaces* **2012**, *4*, 1186−1193.
(41) Gao, W.; Majumder, M.; Alemany, L. B.; Narayanan, T. N.; Ibarra, M. A.; Pradhan, B. K.; Ajayan, P. M. Engineered Graphite Oxide Materials for Application in Water Purification. *ACS Appl. Mater. Interfaces* **2011**, *3*, 1821−1826.
(42) Chandra, V.; Kim, K. S. Highly Selective Adsorption of Hg^{2+} by a Polypyrrole−Reduced Graphene Oxide Composite. *Chem. Commun.* **2011**, *47*, 3942−3944.
(43) Ma, H. L.; Zhang, Y.; Hu, Q. H.; Yan, D.; Yu, Z. Z.; Zhai, M. Chemical Reduction and Removal of Cr(VI) from Acidic Aqueous Solution by Ethylenediamine-Reduced Graphene Oxide. *J. Mater. Chem.* **2012**, *22*, 5914−5916.
(44) Gao, H.; Sun, Y.; Zhou, J.; Xu, R.; Duan, H. Mussel-Inspired Synthesis of Polydopamine-Functionalized Graphene Hydrogel as Reusable Adsorbents for Water Purification. *ACS Appl. Mater. Interfaces* **2013**, *5*, 425−432.
(45) Yang, Y.; Xie, Y.; Pang, L.; Li, M.; Song, X.; Wen, J.; Zhao, H. Preparation of Reduced Graphene Oxide/Poly(acrylamide) Nanocomposite and Its Adsorption of Pb(II) and Methylene Blue. *Langmuir* **2013**, *29*, 10727−10736.
(46) Zhao, G.; Jiang, L.; He, Y.; Li, J.; Dong, H.; Wang, X.; Hu, W. Sulfonated Graphene for Persistent Aromatic Pollutant Management. *Adv. Mater.* **2011**, *23*, 3959−3963.
(47) Zhao, X.; Liu, P. Hydrophobic-Polymer-Grafted Graphene Oxide Nanosheets as an Easily Separable Adsorbent for the Removal of Tetrabromobisphenol A. *Langmuir* **2014**, *30*, 13699−13706.
(48) Ray, S.; Banerjee, B.; Bhaumik, A.; Mukhopadhyay, C. Copper Incorporated Nanorod Like Mesoporous Silica for One Pot Aerobic Oxidative Synthesis of Pyridines. *Catal. Commun.* **2015**, *58*, 97−102.
(49) Machado, B. F.; Serp, P. Graphene-Based Materials for Catalysis. *Catal. Sci. Technol.* **2012**, *2*, 54−75.
(50) Del Valle, E. M. M. Cyclodextrins and Their Uses: a Review. *Process Biochem.* **2004**, *39*, 1033−1046.
(51) Bibby, A.; Mercier, L. Adsorption and Separation of Water-Soluble Aromatic Molecules by Cyclodextrin-Functionalized Mesoporous Silica. *Green Chem.* **2003**, *5*, 15−19.
(52) Bhattarai, B.; Muruganandham, M.; Suri, R. P. S. Development of High Efficiency Silica Coated β-Cyclodextrin Polymeric Adsorbent for the Removal of Emerging Contaminants of Concern from Water. *J. Hazard. Mater.* **2014**, *273*, 146−154.
(53) Guo, Y.; Guo, S.; Ren, J.; Zhai, Y.; Dong, S.; Wang, E. Cyclodextrin Functionalized Graphene Nanosheets with High Supramolecular Recognition Capability: Synthesis and Host Guest Inclusion for Enhanced Electrochemical Performance. *ACS Nano* **2010**, *4*, 4001−4010.
(54) Mondal, A.; Jana, N. R. Fluorescent Detection of Cholesterol Using β-Cyclodextrin Functionalized Graphene. *Chem. Commun.* **2012**, *48*, 7316−7318.
(55) Chen, L.; Dionysiou, D. D.; O'Shea, K. Complexation of Microcystins and Nodularin by Cyclodextrins in Aqueous Solution, a Potential Removal Strategy. *Environ. Sci. Technol.* **2011**, *45*, 2293−2300.
(56) Jana, N. R.; Earhart, C.; Ying, J. Y. Synthesis of Water-Soluble and Functionalized Nanoparticles by Silica Coating. *Chem. Mater.* **2007**, *19*, 5074−5082.

DOI: 10.1021/acsami.5b02038
ACS Appl. Mater. Interfaces 2015, 7, 9911−9919

(57) Hummers, W. S.; Offeman, R. E. Preparation of Graphitic Oxide. *J. Am. Chem. Soc.* **1958**, *80*, 1339−1339.
(58) Dreyer, D. R.; Park, S.; Bielawski, C. W.; Ruoff, R. S. The Chemistry of Graphene Oxide. *Chem. Soc. Rev.* **2010**, *39*, 228−240.
(59) Sinha, A.; Jana, N. R. Nanoparticle-Incorporated Functional Mesoporous Silica Colloid for Diverse Applications. *Eur. J. Inorg. Chem.* **2012**, 4470−4478.
(60) Matilainen, A.; Sillanpaa, M. Removal of Natural Organic Matter from Drinking Water by Advanced Oxidation Processes. *Chemosphere* **2010**, *80*, 351−365.

DOI: 10.1021/acsami.5b02038
ACS Appl. Mater. Interfaces 2015, 7, 9911−9919